Sparse grid approach to accelerate Particle-In-Cell (PIC) methods

M. Chung To Sang[‡], F. Deluzet[†], G. Fubiani [‡], L. Garrigues [‡], C. Guillet[†‡*] , J.Narski[†]

† Institut de Mathématiques de Toulouse (IMT)
‡ Laboratoire Plasma et Conversion d'énergie (LAPLACE)

June 20, 2021

SMAI
société de mathématiques appliquées et industrielles

* Corresponding author

Outline

Introduction

- Topic: simulation of kinetic plasma based on Vlasov-Poisson system.
- **Particle-In-Cell** (PIC) (1950s): most used numerical method for Vlasov-Poisson (coupling between particle approach and grid-based method).
  - Benefits: No velocity grid (reduces the dimension from six to three compared to continuum kinetic methods), simplicity, ease of parallelization, robustness
  - Drawbacks: Need of space grid, slow-converging statistical error, exponential dependence on dimension, number of particles exceedingly large in 3D
- Sparse grids: **combination technique** (1992) (initially for pde's solutions):
  - Benefits: Reduces dimension dependence for grid-based methods
  - Drawbacks: Needs smooth solutions and structured grid
- First application of the combination technique to Particle-In-Cell methods by Ricketson *et al.*[2] (2017)
- Assessment of the method and analyse of the weaknesses in 2D (objective is 3D).

Vlasov Poisson system

Non-relativistic system of **Vlasov-Poisson** with fixed magnetic field **B**:

$$\begin{cases} \dfrac{\partial f_s}{\partial t} + \mathbf{v} \cdot \nabla_{\mathbf{x}} f_s + \dfrac{q_s}{m_s}(\mathbf{E} + \mathbf{v} \times \mathbf{B}) \cdot \nabla_{\mathbf{v}} f_s = 0, \\ \nabla \cdot \mathbf{E} = \dfrac{\rho}{\varepsilon_0}, \qquad \mathbf{E} = -\nabla \Phi, \end{cases} \tag{1}$$

- $f_s(\mathbf{x}, \mathbf{v}, t)$ phase-space distribution attached to the species s.
- $\mathbf{E}$ electric field, Φ electric potential
- ρ charge density obtained from the phase-space distribution of each species:

$$\rho(\mathbf{x}, t) = \sum_s q_s \int f_s(\mathbf{x}, \mathbf{v}, t) d\mathbf{v} \tag{2}$$

Particle-In-Cell scheme

- Coupling between a particle approach for Vlasov equation and mesh-based solver for Poisson equation:

1. f_s represented by a collection of N numerical particles with positions and velocities, denoted $(\mathbf{x}_p, \mathbf{v}_p)$, $p = 1, \ldots, N$ evolving following Newton equations:

$$\frac{d\mathbf{x}_p}{dt} = \mathbf{v}_p, \qquad \frac{d\mathbf{v}_p}{dt} = \frac{q_s}{m_s}(\mathbf{E} + \mathbf{v} \times \mathbf{B})|_{\mathbf{x}=\mathbf{x}_p}. \tag{3}$$

2. ρ projected onto a grid with a numerical convolution kernel and a sum over the particles (see details in the following).

3. $\mathbf{E}$ obtained by resolving the Poisson equation and differenciating Φ on the grid:

$$\Delta_h \Phi_{\mathbf{j}} = -\frac{\rho}{\varepsilon_0}, \qquad \mathbf{E}_{\mathbf{j}} = -\nabla_h \Phi_{\mathbf{j}}, \tag{4}$$

with Δ_h, ∇_h discrete operators on the grid with discretization h.

4. $\mathbf{E}$ evaluated at the particles positions by interpolation.

Particle-In-Cell scheme

- Coupling between a particle approach for Vlasov equation and mesh-based solver for Poisson equation:

1. f_s represented by a collection of N numerical particles with positions and velocities, denoted $(\mathbf{x}_p, \mathbf{v}_p)$, $p = 1, \ldots, N$ evolving following Newton equations:

$$\frac{d\mathbf{x}_p}{dt} = \mathbf{v}_p, \qquad \frac{d\mathbf{v}_p}{dt} = \frac{q_s}{m_s}(\mathbf{E} + \mathbf{v} \times \mathbf{B})|_{\mathbf{x}=\mathbf{x}_p}. \tag{3}$$

2. ρ projected onto a grid with a numerical convolution kernel and a sum over the particles (see details in the following).

3. $\mathbf{E}$ obtained by resolving the Poisson equation and differenciating Φ on the grid:

$$\Delta_h \Phi_{\mathbf{j}} = -\frac{\rho}{\varepsilon_0}, \qquad \mathbf{E}_{\mathbf{j}} = -\nabla_h \Phi_{\mathbf{j}}, \tag{4}$$

with Δ_h, ∇_h discrete operators on the grid with discretization h.

4. $\mathbf{E}$ evaluated at the particles positions by interpolation.

Particle-In-Cell scheme

- Coupling between a particle approach for Vlasov equation and mesh-based solver for Poisson equation:

1. f_s represented by a collection of N numerical particles with positions and velocities, denoted $(\mathbf{x}_p, \mathbf{v}_p)$, $p = 1, \dots, N$ evolving following Newton equations:

$$\frac{d\mathbf{x}_p}{dt} = \mathbf{v}_p, \qquad \frac{d\mathbf{v}_p}{dt} = \frac{q_s}{m_s}(\mathbf{E} + \mathbf{v} \times \mathbf{B})|_{\mathbf{x}=\mathbf{x}_p}. \tag{3}$$

2. ρ projected onto a grid with a numerical convolution kernel and a sum over the particles (see details in the following).

3. $\mathbf{E}$ obtained by resolving the Poisson equation and differenciating Φ on the grid:

$$\Delta_h \Phi_\mathbf{j} = -\frac{\rho}{\varepsilon_0}, \quad \mathbf{E}_\mathbf{j} = -\nabla_h \Phi_\mathbf{j}, \tag{4}$$

with Δ_h, ∇_h discrete operators on the grid with discretization h.

4. $\mathbf{E}$ evaluated at the particles positions by interpolation.

Particle-In-Cell scheme

- Coupling between a particle approach for Vlasov equation and mesh-based solver for Poisson equation:

1. f_s represented by a collection of N numerical particles with positions and velocities, denoted $(\mathbf{x}_p, \mathbf{v}_p)$, $p = 1, \ldots, N$ evolving following Newton equations:

$$\frac{d\mathbf{x}_p}{dt} = \mathbf{v}_p, \qquad \frac{d\mathbf{v}_p}{dt} = \frac{q_s}{m_s}(\mathbf{E} + \mathbf{v} \times \mathbf{B})|_{\mathbf{x}=\mathbf{x}_p}. \tag{3}$$

2. ρ projected onto a grid with a numerical convolution kernel and a sum over the particles (see details in the following).

3. $\mathbf{E}$ obtained by resolving the Poisson equation and differenciating Φ on the grid:

$$\Delta_h \Phi_{\mathbf{j}} = -\frac{\rho}{\varepsilon_0}, \quad \mathbf{E}_{\mathbf{j}} = -\nabla_h \Phi_{\mathbf{j}}, \tag{4}$$

with Δ_h, ∇_h discrete operators on the grid with discretization h.

4. $\mathbf{E}$ evaluated at the particles positions by interpolation.

Errors in Particle-In-Cell scheme

- Considering a leap frog scheme for the advance in time of the particles, a second order centered finite difference scheme for the field solver and the precedent framework for the projection of the density on the grid, the error of the scheme ϵ scales with:

$$\epsilon \sim \Delta t^2, h^2, \underbrace{(Nh^d)^{-1/2}}_{\text{(mean number of particles per cell of the grid)}^{-1/2}}. \tag{5}$$

- Conditions of convergence are:

$$\Delta T \ll 1, \underbrace{h \ll 1, \quad N \gg h^{-d}}_{\text{require an extremely high number of particles}}. \tag{6}$$

→ Slow convergence of the statistical error ($\mathcal{O}(N^{-1/2})$)

→ ϵ depends exponentially on the dimension d of the problem (curse of dimensionality)

Errors in Particle-In-Cell scheme

- Considering a leap frog scheme for the advance in time of the particles, a second order centered finite difference scheme for the field solver and the precedent framework for the projection of the density on the grid, the error of the scheme ϵ scales with:

$$\epsilon \sim \Delta t^2, h^2, \underbrace{(Nh^d)^{-1/2}}_{(\text{mean number of particles per cell of the grid})^{-1/2}}. \tag{5}$$

- Conditions of convergence are:

$$\Delta T \ll 1, \underbrace{h \ll 1, \quad N \gg h^{-d}}_{\text{require an extremely high number of particles}}. \tag{6}$$

→ Slow convergence of the statistical error ($\mathcal{O}(N^{-1/2})$)

→ ϵ depends exponentially on the dimension d of the problem (curse of dimensionality)

Presentation of the combination technique

- **Combination technique** [4]: sparse grid method of interpolation based on representations of a function on anisotropic grids and linear combination:

1. Considering anisotropic grids $\Omega_{\mathbf{l}}$ (***subgrids***) parametrized by an index $\mathbf{l} = (l_1, l_2) \in \mathbb{N}^2$ veryfing $|\mathbf{l}|_1 = n + 1 - \sigma$, for $\sigma = 0, 1$

Figure: Subgrids $\Omega_{(l_1, l_2)}$ for $n = 3$.

2. Sparse grid $f_{\mathbf{l}}^m$ interpolant of degree m constructed on each $\Omega_{\mathbf{l}}$:

$$f_{\mathbf{l}}^m(\mathrm{x}) := \sum_{\mathbf{j} \in \mathcal{J}_{\mathbf{l}}} \alpha_{\mathbf{l},\mathbf{j}} \phi_{\mathbf{l},\mathbf{j}}^m(\mathrm{x}). \tag{7}$$

- $\mathcal{J}_{\mathbf{l}}$: index node set for grid $\Omega_{\mathbf{l}}$, $\phi_{\mathbf{l},\mathbf{j}}^m$ B-spline of degree m centered at grid nodes of index $\mathbf{j}$, $\alpha_{\mathbf{l},\mathbf{j}}$ coefficients verifying interpolation conditions.

Presentation of the combination technique

- **Combination technique** [4]: sparse grid method of interpolation based on representations of a function on anisotropic grids and linear combination:

1. Considering anisotropic grids $\Omega_{\mathbf{l}}$ (***subgrids***) parametrized by an index $\mathbf{l} = (l_1, l_2) \in \mathbb{N}^2$ veryfing $|\mathbf{l}|_1 = n + 1 - \sigma$, for $\sigma = 0, 1$

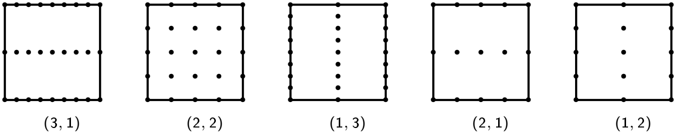

Figure: Subgrids $\Omega_{(l_1, l_2)}$ for $n = 3$.

2. Sparse grid $f_{\mathbf{l}}^m$ interpolant of degree m constructed on each $\Omega_{\mathbf{l}}$:

$$f_{\mathbf{l}}^m(\mathbf{x}) := \sum_{\mathbf{j} \in \mathcal{J}_{\mathbf{l}}} \alpha_{\mathbf{l},\mathbf{j}} \phi_{\mathbf{l},\mathbf{j}}^m(\mathbf{x}). \quad (7)$$

   - $\mathcal{J}_{\mathbf{l}}$: index node set for grid $\Omega_{\mathbf{l}}$, $\phi_{\mathbf{l},\mathbf{j}}^m$ B-spline of degree m centered at grid nodes of index $\mathbf{j}$, $\alpha_{\mathbf{l},\mathbf{j}}$ coefficients verifying interpolation conditions.

Presentation of the combination technique

- **Combination technique** [4]: sparse grid method of interpolation based on representations of a function on anisotropic grids and linear combination:

1. Considering anisotropic grids $\Omega_{\mathbf{l}}$ (***subgrids***) parametrized by an index $\mathbf{l} = (l_1, l_2) \in \mathbb{N}^2$ veryfing $|\mathbf{l}|_1 = n + 1 - \sigma$, for $\sigma = 0, 1$

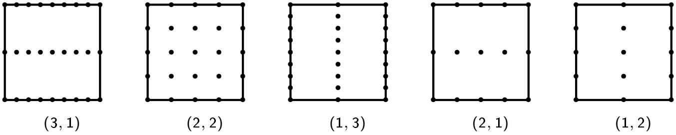

Figure: Subgrids $\Omega_{(l_1, l_2)}$ for $n = 3$.

2. Sparse grid $f_{\mathbf{l}}^m$ interpolant of degree m constructed on each $\Omega_{\mathbf{l}}$:

$$f_{\mathbf{l}}^m(\mathbf{x}) := \sum_{\mathbf{j} \in \mathcal{J}_{\mathbf{l}}} \alpha_{\mathbf{l},\mathbf{j}} \phi_{\mathbf{l},\mathbf{j}}^m(\mathbf{x}). \quad (7)$$

   - $\mathcal{J}_{\mathbf{l}}$: index node set for grid $\Omega_{\mathbf{l}}$, $\phi_{\mathbf{l},\mathbf{j}}^m$ B-spline of degree m centered at grid nodes of index $\mathbf{j}$, $\alpha_{\mathbf{l},\mathbf{l}}$ coefficients verifying interpolation conditions.

Presentation of the combination technique

- **Combination technique** [4]:

3. Sparse grid interpolant constructed **by linear combination** of the partial interpolants of equation (7):

$$f_n^m(\mathrm{x}) := \sum_{|\mathbf{l}|_1=n+1} f_{\mathbf{l}}^m(\mathrm{x}) - \sum_{|\mathbf{l}|_1=n} f_{\mathbf{l}}^m(\mathrm{x}) \qquad (8)$$

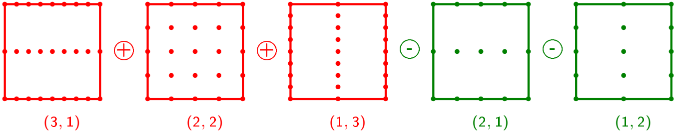

Figure: Combination for n=3.

→ Easily extensible in dimension $d \in \mathbb{N}$ [1].

Combination technique

Theorem (d dimension)

Let f be a smooth function with a pointwise error expression of the form:

$$f(\mathbf{x}) - f_l^m(\mathbf{x}) = \sum_{m=1}^{d} \sum_{\{1,\dots,m\}\subset\{1,\dots,d\}} \tau_{1,\dots,m}(\mathbf{x}\,;h_{l_1},\dots,h_{l_m})h_{l_1}^2 \dots h_{l_m}^2, \qquad (9)$$

with bounded $\|\tau_{1,\dots,m}(\cdot;h_{l_1},\dots,h_{l_m})\|_\infty \leq \kappa$. The sparse grid interpolant of the function converges to the exact solution in L^p-norm:

$$\|f_n^m - f\|_p = \mathcal{O}(\log_2(h_n^{-1})^{d-1}h_n^2), \qquad 1 \leq p \leq \infty, \qquad (10)$$

Proof.

See [1,4]. □

Remark

- Error: $\mathcal{O}(h_n^2)$ (classical) $\rightarrow \mathcal{O}(\log_2(h_n^{-1})^{d-1}h_n^2)$ (sparse)
- Complexity: $\mathcal{O}(h_n^{-d})$ (classical) $\rightarrow \mathcal{O}(\log_2(h_n^{-1})^{d-1}h_n^{-1})$ (sparse)

Projection of the density onto the subgrids (Monte-Carlo)

- Let $\tilde{\mathbf{X}}$ random variable with probability density function $\int \tilde{f}_s(\cdot, \mathbf{v}) d\mathbf{v}$, where $\tilde{f}_s = \frac{q_s}{\mathcal{Q}_s} f_s$, $\mathcal{Q}_s$ the total charge of particles s.

$$\rho(\mathbf{x}) = \mathcal{Q}\mathbb{E}[\delta(\tilde{\mathbf{X}} - \mathbf{x})]. \tag{11}$$

- δ substituted by a **numerical convolution kernel** $\mathcal{S}_d$ based on the cell width of the subgrid h_{l}:

$$\mathcal{S}_{d,\mathrm{l}}(\mathbf{x}) := \prod_{t=1}^{d} \frac{1}{h_{l_t}} \mathcal{S}\left(\frac{x_t}{h_{l_t}}\right), \quad \mathcal{S}(x_t) = \begin{cases} 1 - |x_t|, & \text{if } |x_t| \leq 1, \\ 0, & \text{else.} \end{cases} \tag{12}$$

Figure: Examples of hierarchical shape function $\mathcal{S}_{d,\mathrm{l}}(\mathbf{x} - \mathbf{x}_p)$ in the two dimensional case.

Projection of the density onto the subgrids (Monte-Carlo)

- Let $\tilde{\mathbf{X}}$ random variable with probability density function $\int \tilde{f}_s(\cdot, \mathbf{v}) d\mathbf{v}$, where $\tilde{f}_s = \frac{q_s}{\mathcal{Q}_s} f_s$, $\mathcal{Q}_s$ the total charge of particles s.

$$\rho(\mathbf{x}) = \mathcal{Q}\mathbb{E}[\delta(\tilde{\mathbf{X}} - \mathbf{x})]. \quad (11)$$

- δ substituted by a **numerical convolution kernel** $\mathcal{S}_d$ based on the cell width of the subgrid $h_{\mathbf{l}}$:

$$\mathcal{S}_{d,\mathbf{l}}(\mathbf{x}) := \prod_{t=1}^{d} \frac{1}{h_{l_t}} \mathcal{S}\left(\frac{x_t}{h_{l_t}}\right), \quad \mathcal{S}(x_t) = \begin{cases} 1 - |x_t|, & \text{if } |x_t| \leq 1, \\ 0, & \text{else.} \end{cases} \quad (12)$$

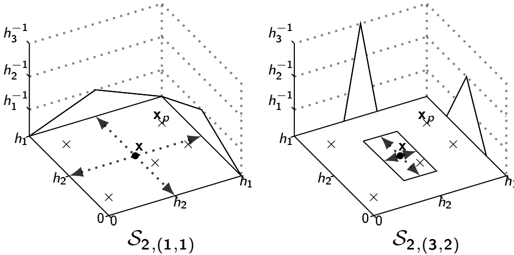

Figure: Examples of hierarchical shape function $\mathcal{S}_{d,\mathbf{l}}(\mathbf{x} - \mathbf{x}_p)$ in the two dimensional case.

Projection of the density onto the subgrids (Monte-Carlo)

- Since position particles are independant realizations of $\tilde{\mathbf{X}}$, we introduce a **statistical estimator** for the density:

$$\rho_{h,N}(\mathbf{x}) := \frac{\mathcal{Q}}{N}\sum_{p=1}^{N}\mathcal{S}_d\left(\frac{\mathbf{x}-\mathbf{x}_p}{h}\right). \tag{13}$$

Projection of the density onto the subgrids

Proposition

Assuming enough smoothness on the probability density $\tilde{f}(\cdot, \mathbf{v}) \in X_4$, MSRE is:

$$\left(\int (\rho_{h,N}(\mathbf{x}) - \rho(\mathbf{x}))^2 d\mathbf{x}_p\right)^{\frac{1}{2}} \leq \text{Bias}(\rho_{h,N}(\mathbf{x})) + \mathbb{V}[\rho_{h,N}(\mathbf{x})]^{\frac{1}{2}}, \quad (14)$$

where the bias and the square root variance are given by:

$$\text{Bias}(\rho_{\mathbf{l},\mathbf{j},N}) = \sum_{m=1}^{d} \sum_{\{1,\ldots,m\}\subset\{1,\ldots,d\}} \tau_{1,\ldots,m}(\mathbf{x}_{\mathbf{l},\mathbf{j}}\,; h_{l_1}, \ldots, h_{l_m}) h_{l_1}^2 \ldots h_{l_m}^2, \quad (15)$$

$$(\mathbb{V}[\rho_{\mathbf{l},\mathbf{j},N}])^{\frac{1}{2}} = \mathcal{O}\left((N h_{n+1-\sigma})^{-\frac{1}{2}}\right), \quad (16)$$

Proof.

See [1, 5]. □

Remark

- The bias expression (15) verifies the assumption of equation (9) in the combination technique theorem.
- Statistical error reduction : $(N h_{n+1-\sigma})^{-\frac{1}{2}} < (N h_n^d)^{-\frac{1}{2}}, \quad \sigma = 0, \ldots, d-1$

Subgrid Particle-In-Cell scheme

- ρ projected onto each subgrid $\Omega_{\mathbf{l}}$, $\mathbf{E}$ solved on each subgrid and interpolated at particle positions with combination technique:

$$\mathbf{E}_n^m(\mathbf{x}_p) := \sum_{|\mathbf{l}|_1=n+1} \mathbf{E}_{\mathbf{l}}^m(\mathbf{x}_p) - \sum_{|\mathbf{l}|_1=n} \mathbf{E}_{\mathbf{l}}^m(\mathbf{x}_p), \tag{17}$$

  with $\mathbf{E}_{\mathbf{l}}^m(\mathbf{x}_p)$ the sparse grid interpolant of the electric field on the subgrid $\Omega_{\mathbf{l}}$.

- Noise reduction (ρ projected onto grids with larger cells) and acceleration of the resolution of the electric field (complexity falls from $\mathcal{O}(h_n^{-d})$ to $\mathcal{O}(\log_2(h_n^{-1})^{d-1} h_n^{-1})$).

Convergence of the sparse grid interpolant

Theorem (Convergence of the electric field interpolant)

Assuming enough smoothness on ρ so that $\Phi \in X_{5,0}(\gamma)$, $\rho \in X_5(\kappa)$, the sparse grid interpolant of the electric field converges to the exact solution in L^p-norm:

$$\|\boldsymbol{E}_n^m - \boldsymbol{E}\|_p = \mathcal{O}\left(\log_2(h_n^{-1})^{d-1}\left(h_n^2 + (Nh_n)^{-\frac{1}{2}}\right)\right), \quad 1 \leq p \leq \infty, \qquad (18)$$

where $\boldsymbol{E} = -\nabla\Phi$, $\Delta\Phi = -\rho/\varepsilon_0$.

Proof.

See [1]. □

Remark

- The statistical error scales with $\log_2(h_n^{-1})^{d-1}(Nh_n)^{-\frac{1}{2}}$ in comparison to $(Nh_n^d)^{-\frac{1}{2}}$ for the standard PIC method.
- Strong dependance on cross derivatives of the solutions in estimation (18)

Alternatives

- Alternatives in order to alleviate the cross derivative dependances:
  - Offset combination technique [1] inspired from the truncated combination technique [3, 6] where fewer subgrids are considered in the combination
  - Correction of the Subgrid scheme with an enhancement of the subgrids at the resolution of the electric field (Enhanced Subgrid PIC scheme [1])
  - Other alternatives proposed in [1].

Numerical results

- Diocotron instability (2D): Not favorable to sparse grid techniques (non-aligned with the grid structures arising in the simulation, high cross derivatives terms).
  - Electrons immersed in a uniform, immobile, background of ions
  - Fixed magnetic field $\mathbf{B} = (0, 0, B_z)$
  - Deformation of the initially axisymmetric electron density distribution, leading, to the formation of vortices

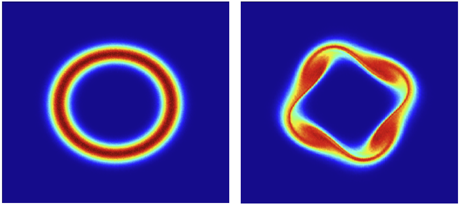

Figure: Diocotron instability. Electron charge density at $t = 0$ (left), $t = T_1$ (right).

Numerical results

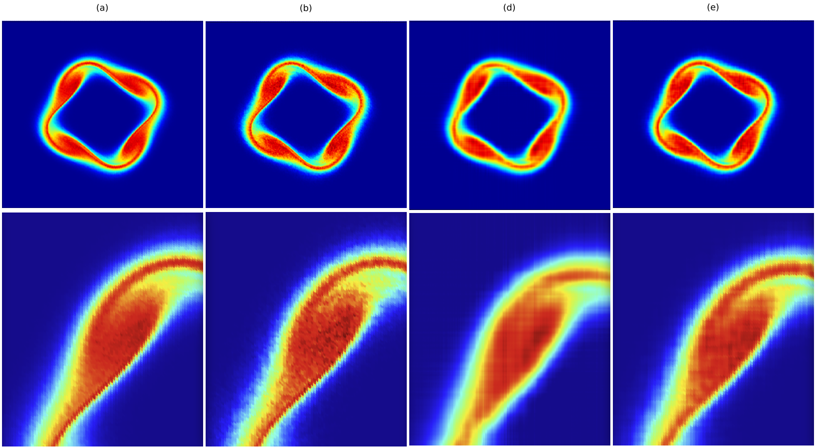

Figure: Standard PIC $P_c = 200$ (a) Standard PIC, $P_c = 40$ (b), Subgrid $P_c = 40$ (d), Enhanced Subgrid (offset) $P_c = 40$ (e). Grid resolution 256×256 cells (a), (b), (e) / 1024×1024 cells (d).

- Subgrid scheme (d):

  ⊕ $\approx$ 11 times less total particles in the simulation
  ⊕ Acceleration of the resolution of electric field
  ⊖ Higher spatial discretization required (strong dependance on cross derivatives of the solution)
  ⊖ Fails to reproduce fine-scale structure.

- Enhanced Subgrid scheme (offset) (e):

  ⊕ $\approx$ 7.25 times less total particles in the simulation
  ⊕ Acceleration of the resolution of electric field
  ⊕ Same spatial discretization
  ⊕ Reproduces correctly the fine-scale structure.

Conclusions

- ⊕ Reduction of the total number of particles + reduction of the complexity of the Poisson equation
- ⊖ Stronger dependence on the high order cross derivatives of the solution (compensated by the alternatives)
- Interest of the method **significantly higher** in dimension 3.

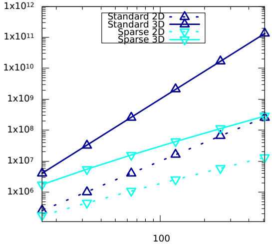

Figure: Total number of particles N as function of the grid resolution.

- Perspectives:
  - Assessment of the method and alternative methods on "more physical" test cases in dimension 2.
  - implementation and optimisation of performance in term of computational time and memory storage in dimension 3

References

M. Chung To Sang, F. Deluzet, G. Fubiani, L. Garrigues, C. Guillet, J.Narski, Sparse Grid interpolation for Particle-In-Cell.

L. F. Ricketson, A. J. Cerfon, Sparse grid techniques for particle-in-cell schemes, Plasma Physics and Controlled Fusion 59 (2) (2016) 024002.

S.Muralikrishnan, A. J. Cerfon, M. Frey, L. F. Ricketson, A. Adelmann, Sparse grids adaptative noise reduction strategy for Particle-In-Cell schemes, Journal of Computational Physics (2020).

M.Griebel, The combination technique for the sparse grid solution of pde's on multiprocessor machines Parallel Process (1992). Lett. 2 61–70.

E.Sonnendrücker, Numerical Methods for the Vlasov-Maxwell equations (2015).

J. Benk, D. Pflüger, Hybrid parallel solutions of the Black-Scholes PDE with the truncated combination technique, in: 2012 International Confer- ence on High Performance Computing and Simulation (HPCS), IEEE, 2012, pp. 678–683.

Appendix

- Number of particles per cell (2D) defined for the regular Particle-In-Cell method (19) and the sparse grid one (20) :

$$P_c = \frac{N}{h_n^{-2} L^2} = N 2^{-2n}, \tag{19}$$

$$P_c = \frac{N}{n h_{n+1}^{-1} L + (n-1) h_n^{-1} L} = \frac{N 2^{-n}}{3n-1}. \tag{20}$$

- Combination technique in dimension $d \in \mathbb{N}$:

$$f_n^m(\mathbf{x}) := \sum_{\sigma=0}^{d-1} (-1)^\sigma \binom{d-1}{\sigma} \sum_{\mathbf{l} \in \mathcal{L}(n,\sigma)} \sum_{\mathbf{j} \in \mathcal{J}_\mathbf{l}} \alpha_{\mathbf{l},\mathbf{j}} \phi_{\mathbf{l},\mathbf{j}}^m(\mathbf{x}), \tag{21}$$

with

$$\mathcal{L}(n,\sigma) := \{\mathbf{l} \in \mathbb{N}^d \mid |\mathbf{l}|_1 = n + d - 1 - \sigma, \ \mathbf{l} \geq (1, ..., 1)\}, \tag{22}$$

Appendix: Outline of the scheme

1. Particles represented and evolved like in equation (3).

2. ρ projected onto each subgrid $\Omega_{\mathbf{l}}$, $|\mathbf{l}|_1 = n + d - 1 - \sigma$, for $\sigma = 0, \dots, d-1$ with the hierarchical estimator defined in equation (13).

3. $\mathbf{E}$ resolved on each subgrid $\Omega_{\mathbf{l}}$ from Poisson equation and by differenciation:

$$\mathbf{E}_{\mathbf{l},\mathbf{j}} = -\nabla_{h_{\mathbf{l}}} \Phi_{\mathbf{l},\mathbf{j}}, \quad \Delta_{h_{\mathbf{l}}} \Phi_{\mathbf{l},\mathbf{j}} = -\frac{\rho_{\mathbf{l},\mathbf{j},N}}{\varepsilon_0}, \tag{23}$$

   with $\nabla_{h_{\mathbf{l}}}$, $\Delta_{h_{\mathbf{l}}}$ discrete second order finite difference operators defined on $\Omega_{\mathbf{l}}$ and depending on the subgrid discretization $h_{\mathbf{l}}$.

4. $\mathbf{E}$ evaluated at particle positions using the combination technique:

$$\mathbf{E}_n^m(\mathbf{x}_p) := \sum_{|\mathbf{l}|_1 = n+1} \mathbf{E}_{\mathbf{l}}^m(\mathbf{x}_p) - \sum_{|\mathbf{l}|_1 = n} \mathbf{E}_{\mathbf{l}}^m(\mathbf{x}_p), \tag{24}$$

   with $\mathbf{E}_{\mathbf{l}}^m(\mathbf{x}_p)$ the sparse grid interpolant of the electric field on the subgrid $\Omega_{\mathbf{l}}$.

Appendix: Total momentum preservation

Theorem (Total momentum)

Assuming periodic boundary conditions, B1-splines for the combination technique, the scheme does preserve the total momentum of the system, i.e

$$\frac{d\mathcal{P}}{dt} = 0, \tag{25}$$

where $\mathcal{P} = m \iint \boldsymbol{v} f_N(\boldsymbol{x}, \boldsymbol{v}, t) d\boldsymbol{x} d\boldsymbol{v}$ *is the total momentum.*

Proof.

See [1]. □

Appendix: Non-linear Landau damping (25 times less particles)

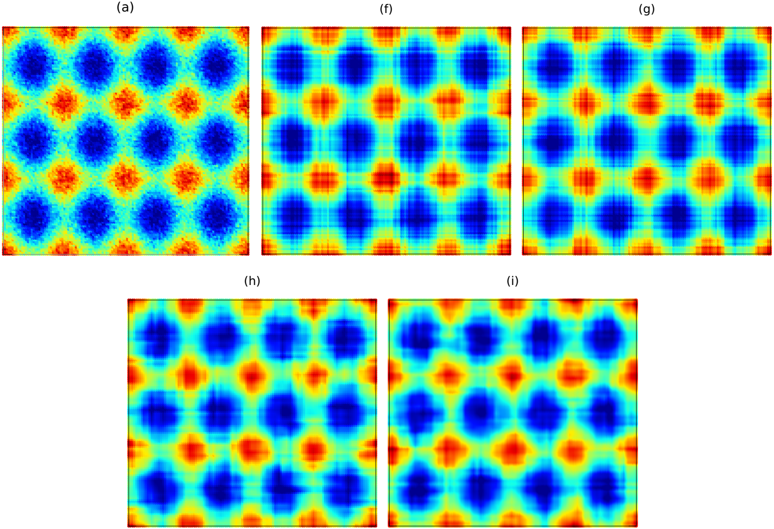

Figure: STD (a), HG (classical) (f), SG (classical) (g), ESG (offset) (h), OHG (offset) (i) schemes. $P_c = 1000$ (a), $P_c = 250$ (f), (g), (h), (i) .